metals

MDPI

Article

Effects of Yttrium on Microstructure Stability and Tensile Properties of China Low Activation Martensitic Steel

Guoxing Qiu [1,2], Dongping Zhan [2,*], Changsheng Li [1], Min Qi [1], Yongkun Yang [2], Zhouhua Jiang [2] and Huishu Zhang [3]

1 State Key Laboratory of Rolling and Automation, Northeastern University, Shenyang 110819, China; guoxingqiu2008@126.com (G.Q.); lics@ral.neu.edu.cn (C.L.); qiminde@126.com (M.Q.)
2 School of Metallurgy, Northeastern University, Shenyang 110819, China; yangyongkun88@163.com (Y.Y.); jiangzh@smm.neu.edu.cn (Z.J.)
3 School of Metallurgy Engineering, Liaoning Institute of Science and Technology, Benxi 117004, China; huishu_zhang@163.com
* Correspondence: zhandp1906@163.com; Tel.: +86-024-8368-7723

Received: 18 March 2019; Accepted: 11 April 2019; Published: 16 April 2019



Abstract: This study investigated the microstructural stability and mechanical properties exhibited by China low activation martensitic (CLAM) steels with different yttrium (Y) contents over 3000 h of aging at 550 °C. Scanning electron microscopy, electron backscatter diffraction analysis, and transmission electron microscopy were employed to investigate the microstructural evolution of the steels. Results indicated that grain boundary migration was slow and the Laves phase precipitation was delayed in Y-containing steels. Grain boundaries at different angles in 0Y and 6Y CLAM steels were significantly affected, and those in 36Y and 71Y alloys exhibited negligible changes during the long-term thermal aging. Moreover, Y contents had appreciable effects on the strength and toughness of the aged steels. The stable microstructure of Y-containing CLAM alloys is responsible for improved strength and impact toughness during aging.

Keywords: CLAM steel; aging; microstructure; mechanical property; DBTT

1. Introduction

Reduced activation ferrite/martensitic (RAFM) steels with 9 wt.% Cr are the most promising structural materials for use in future fusion reactors because of their good thermomechanical properties and creep resistance at high temperatures [1–3]. RAFM steels with guaranteed low activation have been developed by replacing Nb and Mo in conventional 9Cr–FM steels with low-activated Ta and W [4,5]. Numerous countries have developed their own RAFM steels [6,7], such as Eurofer97 (Europe), F82H (Japan), 9Cr–2WVTa (USA), and China low activation martensitic steel (CLAM) (China). CLAM, 9Cr–1.5W–0.2V–0.15Ta, was developed by the Institute of Plasma Physics, Chinese Academy of Sciences (ASIPP), and other institutes and universities [8]. The smelting process [9], mechanical properties [10], compatibility with liquid LiPb [11], and further research and development [12] of CLAM have been evaluated by the ASIPP.

Rare earth (RE) elements have become an important additive in the metallurgical industry, being used as deoxidizers, desulfurizers, modifiers, and alloying elements because of their 4f electron characteristic, alternation valence, large atomic size, and enhanced chemical activity [13]. Numerous studies have focused on the RE element cerium [14]. Another RE element, yttrium (Y), shares similarities with cerium while also possessing unique characteristics [15]. In addition, Y_2O_3 and Y are widely used in strengthening phases in oxide dispersion-strengthened (ODS) alloys [16]. The addition of 0.2 wt.% Y

can result in the refinement of the martensitic lath structure and grain size of CLAM steel [17]. Shi and Han [18] reported that the tensile strength of RAFM steel improved when dislocation movement was effectively hindered by micron-sized Y_2O_3. The effect of trace (<0.1%) Y addition on CLAM steel was evaluated previously [19]. The thermal aging property shown by nuclear power steels during exposure to operating temperatures is important for ensuring the safe operation of nuclear power plants. However, research on the thermal aging property of Y-containing CLAM alloy remains limited. The upper limit temperature of the CLAM steel used in breeding blankets has been proposed as 550 °C. In this study, the microstructural evolution and mechanical properties of Y-containing CLAM alloys subjected to long-term aging at 550 °C were investigated.

2. Materials and Methods

Four CLAM alloys with different Y contents were prepared through a vacuum induction melting process. The chemical compositions of the alloys are shown in Table 1. The alloys were named 0Y, 6Y, 36Y, and 71Y on the basis of their Y content. Ingots were first forged into 35 mm × 50 mm plates, and then hot rolled into 12 mm thick plates. The plates were normalized at 1050 °C for 0.5 h, and then tempered at 750 °C for 1.5 h. All samples were cooled in air. The thermal aging property of Y-containing CLAM alloys exposed at 550 °C for 3000 h under air atmosphere was investigated.

Table 1. Chemical composition of the investigated China low activation martensitic (CLAM) alloys (wt.%).

Alloy	C	Cr	Mn	Si	W	V	S	Ta	P	N	O	Y
0Y	0.11	9.3	0.45	0.05	1.36	0.22	0.010	0.072	0.0085	0.0023	0.0060	-
6Y	0.11	9.4	0.46	0.05	1.35	0.22	0.007	0.071	0.0086	0.0023	0.0054	0.006
36Y	0.11	9.4	0.45	0.05	1.35	0.21	0.004	0.073	0.0084	0.0022	0.0050	0.036
71Y	0.11	9.4	0.45	0.05	1.35	0.22	0.003	0.071	0.0084	0.0022	0.0050	0.071

Samples for testing were spark-machined from aged plates along the rolling direction. A layer with a thickness of more than 2 mm was removed from the surface of each specimen to eliminate the influence of oxidation on thermal aging properties. Specimens for optical microscopy (Leica, Solms, Germany) and scanning electron microscopy (SEM) (ZEISS, Jena, Germany) were etched with vilella reagent (100 mL of alcohol + 5 mL of picric acid + 1 g of muriatic acid). The average prior grain sizes (APGZ) of the steels were measured using the linear intercept method. Transmission electron microscope (TEM) (FEI, Hillsboro, OR, USA) specimens were first mechanically polished to be 30–50 μm thick. Then, a thin disk with a diameter of 3 mm was subjected to twin-jet polishing with an electrolyte solution (95% acetic acid + 5% perchloric acid) at room temperature (RT). Rod specimens with a diameter of 5.0 mm and a length of 25.0 mm were used to test strength at RT. Dog-bone-shaped flat specimens (6.0 mm × 2.0 mm × 30 mm) were used for testing at 550 °C, 600 °C, and 650 °C. Tensile tests were performed with a cross-head speed of 2 mm/min. Full-sized V-notch Charpy specimens (10 mm × 10 mm × 55 mm) were prepared for impact tests over a temperature range of −130 to 25 °C. All tensile tests were performed three times, and the results were averaged. The schematics of the specimens are shown in Figure 1.

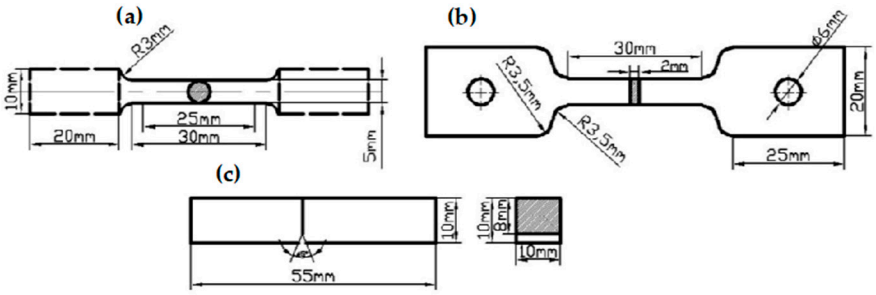


Figure 1. Schematics of the specimens: (**a**) rod specimens; (**b**) dog-bone-shaped flat specimens; and (**c**) full-sized V-notch Charpy specimens.

3. Results and Discussion

3.1. Grain Structural Characteristics

3.1.1. Microstructure

The microstructures of the CLAM alloys after long-term aging are presented in Figure 2. The original heat-treated matrix [19] remained unchanged after aging at 550 °C for 3000 h. Martensitic lath was present in all samples. Table 2 shows the APGZ of the aged samples measured through the linear intercept method. Grains coarsened during the 3000 h of aging but were refined through the hindrance of grain boundaries by Y-containing inclusions, as previously confirmed [19]. The lower coarsening rate of the CLAM steel with 0.071 wt.% Y (11.6 → 13.1 μm) as compared to that of the reference base steel (0Y alloy) (14.7 → 16.9 μm) was attributed to the pinning of the Y inclusions [19]. Surface energy is the driving force of grain boundary migration [20]. Thus, grain coarsening during the 3000 h of aging was a spontaneous process.

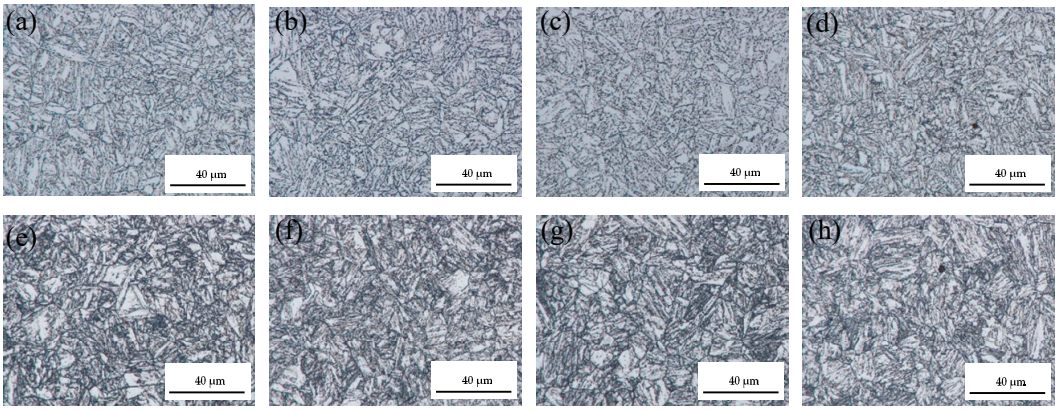


Figure 2. Microstructure of aged samples: (**a**–**d**) 1500 h, (**e**–**h**) 3000 h, (**a**,**e**) 0Y, (**b**,**f**) 6Y, (**c**,**g**) 36Y, and (**d**,**h**) 71Y.

Table 2. Average prior grain sizes (APGZ) of the aged alloys (μm).

Alloys	0 h	1500 h	3000 h
0Y	14.7 (σ = 3.23)	15.6 (σ = 3.42)	16.9 (σ = 3.27)
6Y	14.3 (σ = 3.01)	15.2 (σ = 3.07)	16.3 (σ = 3.12)
36Y	11.7 (σ = 2.23)	12.9 (σ = 2.34)	13.2 (σ = 2.54)
71Y	11.6 (σ = 2.13)	12.0 (σ = 2.04)	13.1 (σ = 2.46)

3.1.2. Precipitations

Additional microstructural details were investigated through back-scattered electron imaging (BSE). New kinds of phases were observed on grain boundaries in the 0Y alloy that had been aged for

1500 h. These phases are marked with black arrows in Figure 3a. The inclusion of elemental Fe, Cr, and W in the phases (Figure 3i) was indicative of the Laves phase ($(Fe, Cr)_2W$) observed in other aged RAFM steels [21]. Laves phases were almost absent from Y-containing CLAM steels aged at 550 °C for 1500 h (Figure 3b–d). The atomic radius of Y, an RE element, is approximately 40% larger than that of Fe atoms. Therefore, the tendency of Y to occupy vacancies, dislocations, phase interfaces, grain boundaries, and other defects upon addition to steel reduces the free energy of the system [22,23]. The segregation of RE elements at grain boundaries would hinder the segregation of elemental W, Cr, and C at grain boundaries and affect the nucleation and precipitation of second phases by considerably affecting the solubility of other alloying elements at grain boundaries [22,23]. The solubility of RE elements would increase when additional RE elements are added, while the carbide nucleation would intensify. The presence of residual Y-rich inclusions in the 71Y alloy would destroy the continuity of the matrix and degrade the mechanical property of the alloy [19,24], as shown in Figure 3d. Several Laves phases appeared in the Y-added CLAM steels and the number of Laves phases in the 0Y alloy increased (Figure 3e–h) when the exposure time was extended to 3000 h.

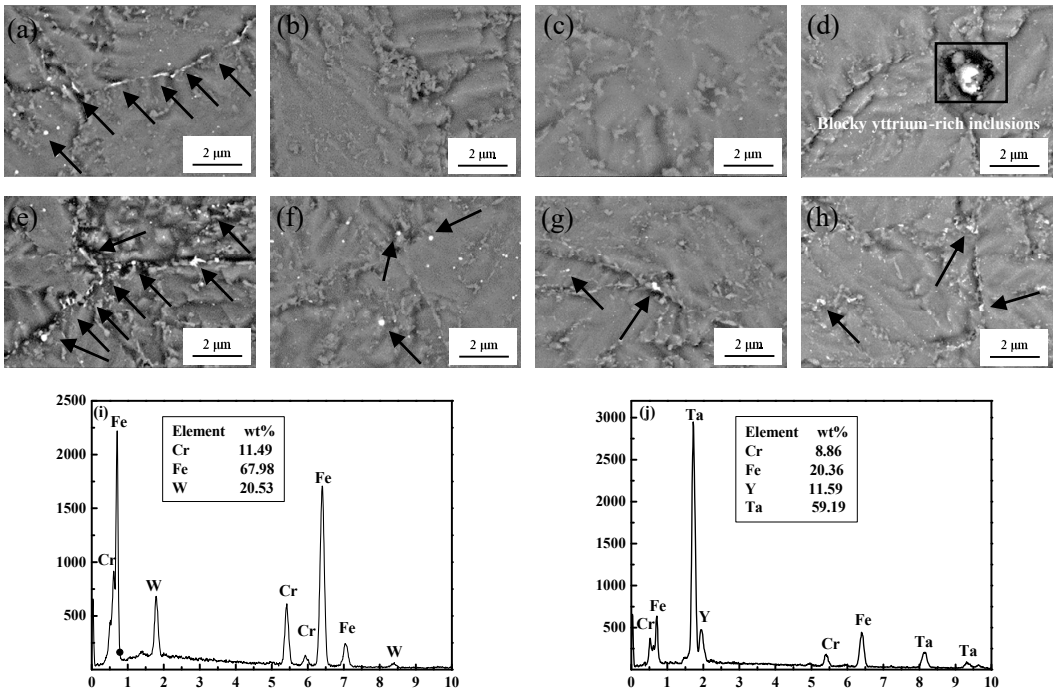


Figure 3. Back-scattered electron (BSE) images of aged samples: (**a**–**d**) 1500 h, (**e**–**h**) 3000 h, (**a**,**e**) 0Y, (**b**,**f**) 6Y, (**c**,**g**) 36Y, and (**d**,**h**) 71Y. (**i**,**j**) EDS spectrum of Laves phase (**i**) and Y-rich inclusions (**j**).

The details of the microstructures of the CLAM steels were revealed through TEM (Figure 4). Martensitic lath boundaries were observed in the aged samples. This observation corresponds with the observation inferred from SEM images (Figure 3). The tempered martensitic microstructure did not show any changes except for lath coarsening during aging at 550 °C. The widths of the lath martensite in the aged alloys are shown in Table 3. Block widths increased by 24.1% (0.29 → 0.36 μm) in the 36Y alloy, by 70.3% (0.37 → 0.63 μm) in the 0Y alloy, by 28.6% (0.28 → 0.36 μm) in the 6Y alloy, and by 36.4% (0.33 → 0.47 μm) in the 71Y alloy. Grain boundaries gradually evolved during the 3000 h of aging. Lath coarsening is a process of dislocation motion and annihilation, and the prolongation of aging time could increase this [25]. The boundary of the martensite lath could have coarsened with time, but significant evidence for the evolution of martensitic lath into sub-grains was not obtained because of the low aging temperature [26]. Meanwhile, precipitates on grain boundaries and inside grains increased after aging. Numerous inhomogeneous spherical, rod, and ellipsoid $M_{23}C_6$ carbides could be found on prior austenite grain and martensitic lath boundaries. The nucleation and growth

of $M_{23}C_6$ carbides were controlled by interfacial energy and the segregation of Cr and C elements. The reduction in the interfacial energy of grain boundaries by RE elements that had segregated at boundaries could inhibit the segregation of elemental Cr. Meanwhile, the activity of elemental C could be reduced, and the solution of elemental C could be promoted by RE elements. The precipitation of $M_{23}C_6$ carbides were inhibited by elemental Y as a result. The carbide content of CLAM steels with Y was lower than that of 0Y alloy, as shown in Figure 4. However, a large number of carbides were observed on the grain boundaries of alloys with Y after 3000 h of exposure at 550 °C.

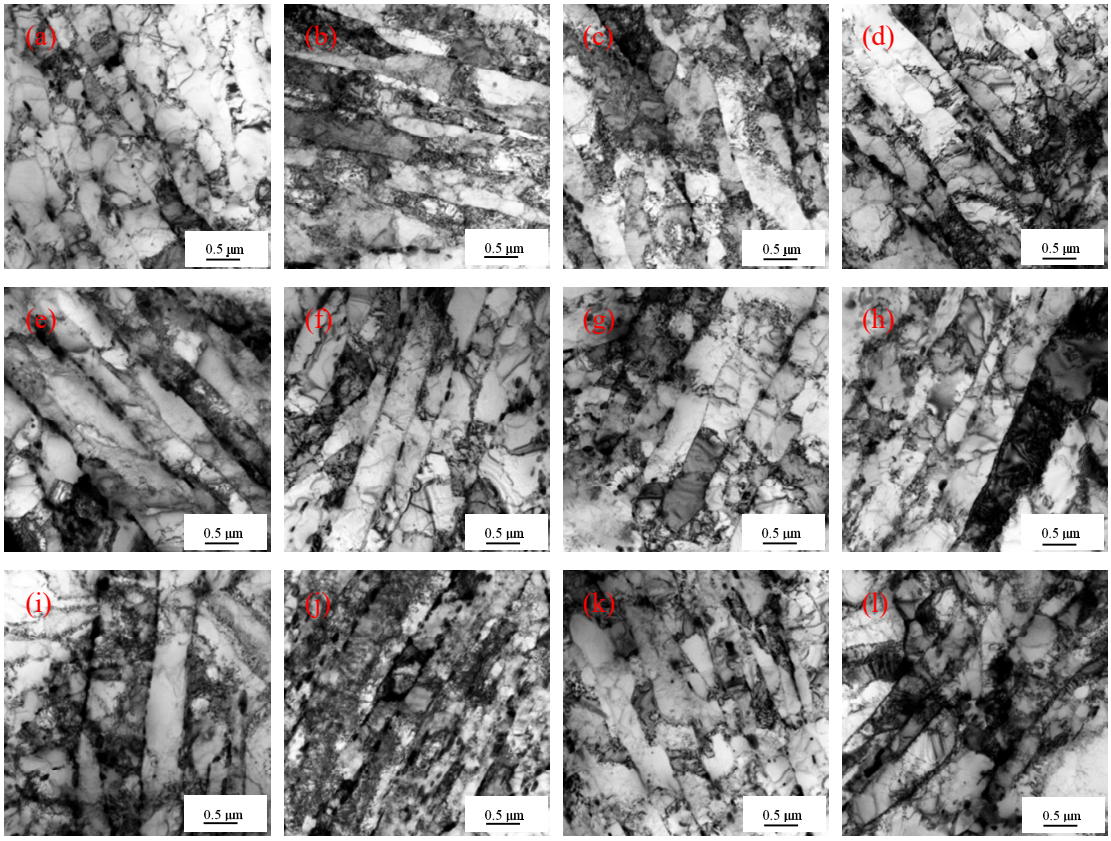


Figure 4. TEM images of the microstructure of CLAM steels: (**a**–**d**) 0 h, (**e**–**h**) 1500 h, (**i**–**l**) 3000 h, (**a**,**e**,**i**) 0Y, (**b**,**f**,**j**) 6Y, (**c**,**g**,**k**) 36Y, and (**d**,**h**,**l**) 71Y.

Table 3. Width of the martensite lath in steels aged for different durations (μm).

Samples	0Y	6Y	36Y	71Y
0 h	0.37	0.28	0.29	0.33
1500 h	0.47	0.34	0.35	0.44
3000 h	0.63	0.36	0.36	0.47

Figure 5 shows the distribution of the misorientation angles in CLAM steels during aging. The angles were mainly less than 10° and ranged from 50 to 60°. The presence of a maximum peak that was less than 5° indicated that sub-grain boundaries and lath boundaries were the main boundaries in the CLAM steels. The same results were reported for CLAM steel that had been aged at 550 °C for 10,000 h [27], and 9Cr–ODS steel that had been aged at 700 °C for 10,000 h [28]. In the present study, grain boundary angles that were less than 10° were defined as low-angle grain boundaries (LABs) and those that were greater than 10° were defined as high-angle grain boundaries (HABs). Long-term thermal aging had a drastic effect on the percentages of grain boundaries with different angles, particularly 4–10° LABs and 50–60° HABs, in 0Y and 6Y CLAM steels. The misorientation angle distributions of 36Y and 71Y alloy exhibited negligible changes during aging. Table 4 shows the

statistical results for misorientation angles in the alloys. Wang et al. [29] and Karthikeyan et al. [30] classified original austenite grain boundaries in martensitic steels as HABs, and sub-grain and martensite lath boundaries as LABs. The increase in the proportion of LABs indicated that sub-grains gradually formed during aging at 550 °C. The coarsening and growth of austenite grains would be responsible for the reduction in HABs in steel during aging and the reduction of the unit volume of HABs. The same result could be inferred from the TEM images (Figure 4) and the statistical results for average grain sizes shown in Table 2.

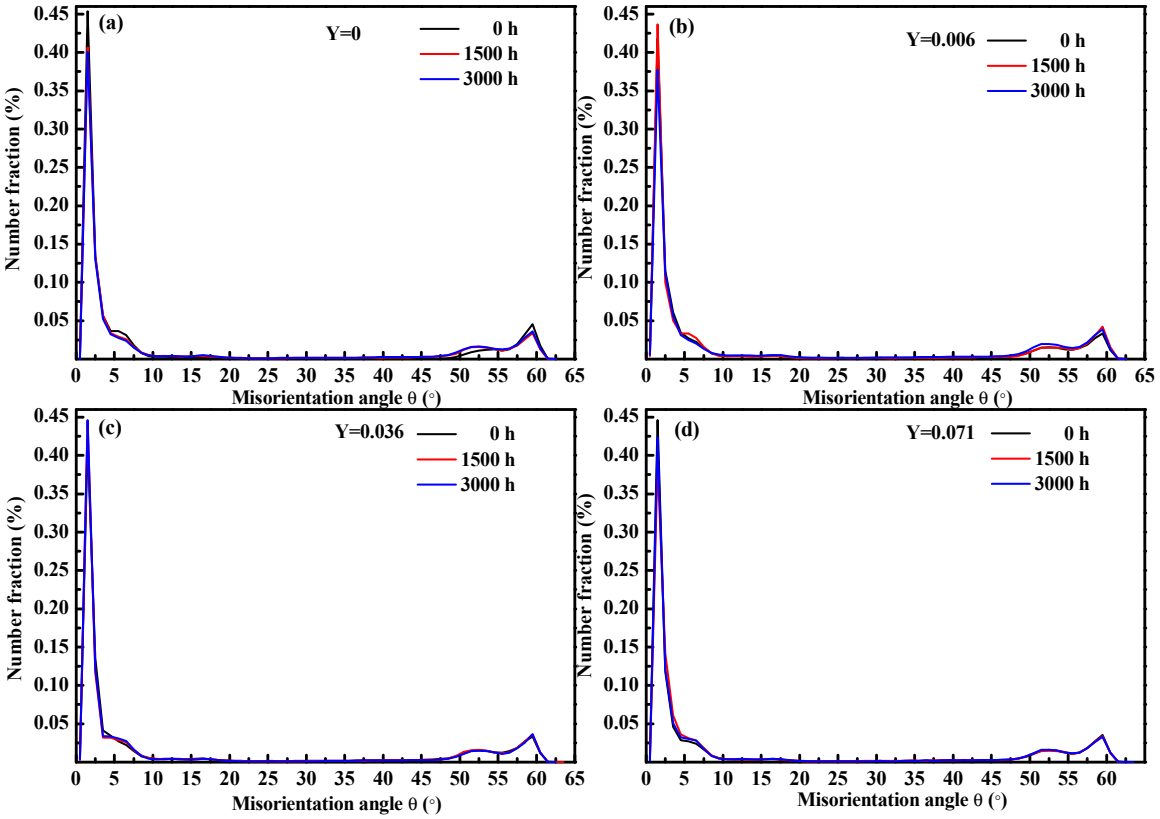


Figure 5. Distribution of misorientation angles in alloys during aging: (**a**) 0Y, (**b**) 6Y, (**c**) 36Y, (**d**) 71Y.

Table 4. Statistical results for misorientation angles in alloys.

Aging Time	0Y		6Y		36Y		71Y	
	HABs	LABs	HABs	LABs	HABs	LABs	HABs	LABs
0 h	0.215	0.785	0.286	0.714	0.286	0.714	0.272	0.728
1500 h	0.277	0.723	0.293	0.717	0.285	0.715	0.273	0.727
3000 h	0.300	0.700	0.351	0.659	0.271	0.719	0.277	0.723

3.2. Tensile Test

Tensile Properties

The tensile properties of the alloys at room temperature are shown in Table 5. The yield strength (YS) of the alloys at 550 °C, 600 °C, and 650 °C is plotted in Figure 6. The YS and ultimate tensile strength of the 0Y alloy first increased and then decreased with the prolongation of aging time at RT, as shown in Table 5. The increment in YS could be attributed to the precipitation of Laves phases, and the decrement in YS could be attributed to the coarsening of carbides and grains. For the steels with Y, YS first decreased and then held the line with a small fluctuation. Grain coarsening dominated during the early aging stage, and carbide precipitation mainly accounted for the fluctuation observed

later in the aging stage. The trends shown by the changes in the YS of the 0Y alloy with aging time remained consistent as the test temperature increased. A temperature inflection point (600 °C) existed for the 36Y and 71Y steels. The YS first increased and then remained consistent because of the reduction in sub-grains at 600 °C. In contrast to the low-temperature stage (<600 °C), the precipitation of the second phase dominated in this stage (≥600 °C). The inclusions in Y-CLAM alloys were mainly Fe–Cr–Y–Ta–S–O, which act as strengthening particles in the steel [18,19,24]. These results indicate that the addition of Y affected the precipitation of carbides.

Table 5. Tensile properties of the alloys at room temperature (MPa).

Alloy	0 h [19]		1500 h		3000 h	
	$R_{0.2}$	R_m	$R_{0.2}$	R_m	$R_{0.2}$	R_m
0Y	548.2 ± 3.5	655.1 ± 2.4	566.5 ± 3.2	683.4 ± 3.2	551.4 ± 2.5	675.3 ± 2.2
6Y	571.4 ± 4.6	699.3 ± 4.6	528.4 ± 3.6	666.4 ± 3.0	532.6 ± 3.5	681.5 ± 3.7
36Y	598.6 ± 4.5	718.6 ± 4.7	551.0 ± 3.5	672.9 ± 3.3	555.2 ± 3.0	674.6 ± 4.3
71Y	552.2 ± 5.7	663.3 ± 6.5	494.7 ± 2.7	645.8 ± 2.5	501.7 ± 3.4	652.9 ± 4.0

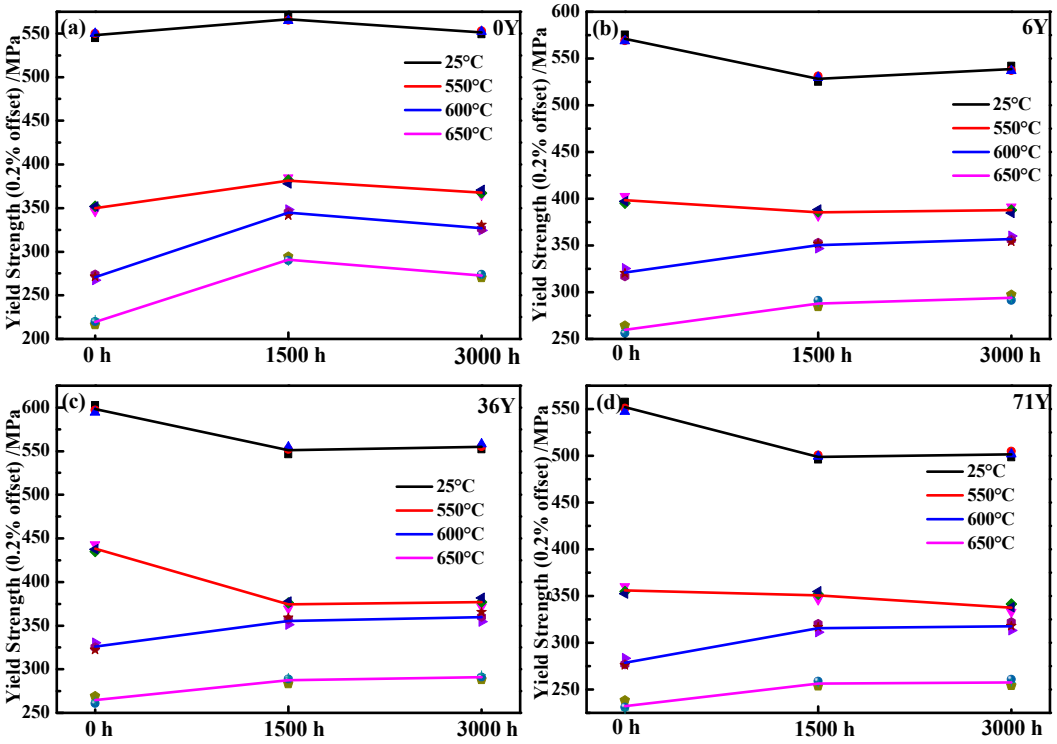


Figure 6. Tensile properties of the steels vs. temperature: (**a**) 0Y, (**b**) 6Y, (**c**) 36Y, (**d**) 71Y.

3.3. Charpy Impact Properties

The absorbed impact energy values of the aged alloys are shown in Figure 7. The Boltzmann function ($A_{KV} = \frac{A_1 - A_2}{1+\exp[(T-x_0)/\Delta x]}$, where x_0 is the ductile–brittle transition temperature) was used to fit the impact curves to obtain the ductile–brittle transition temperature (DBTT). The DBTT of the steels are shown in the upper left-hand side of Figure 7. The impact curve exhibited two distinct regimes. The upper shelf regime (USR) ranged from −20 to 25 °C. The DBTT drastically increased and the USR decreased with aging. Cleavage crack propagation was retarded or deviated because of the high grain boundary area per unit volume attributed to small grain sizes. The 36Y alloy showed a grain size that could improve toughness under the same aging time. Crack propagation could be effectively retarded or deflected by HABs, such as martensitic lath boundaries. The grain size of the steels increased by

approximately 2.3, 2.0, 1.5, and 1.5 μm during the 3000 h of aging at 550 °C, as shown in Table 2. The relationship between DBTT and grain size could be expressed as follows [27]:

$$\alpha \times DBTT = \beta - \ln\left(d_{eff}\right)^{-1/2},$$

where α and β are material constants, and d_{eff} is the effective grain size. This relationship indicates that DBTT increased as the effective grain size increased.

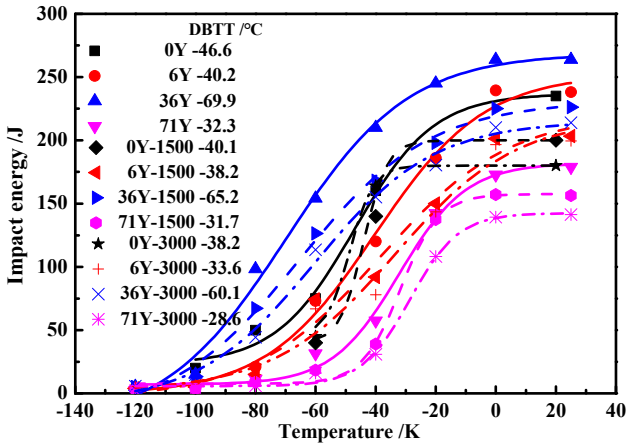


Figure 7. Impact absorbed energy of the aged alloys.

The presence of the Laves phase during aging would be another important reason for the reduction in USR and increase in DBTT.

4. Conclusions

The microstructural stability and mechanical properties exhibited by CLAM steels with different Y contents over 3000 h of aging at 550 °C were investigated. The following conclusions were obtained:

(1) Long-term thermal aging drastically affected the percentages of grain boundaries at different angles in 0Y and 6Y CLAM steels. This effect indicates that sub-grains formed in the alloys during aging for 3000 h.

(2) The addition of elemental Y could improve microstructural and carbide stability. The mechanical properties of 6Y and 36Y alloys were better than those of 0Y steel. However, residual blocky Y-rich inclusions in 71Y alloy could degrade the performance of the aged alloy.

(3) The precipitation of the Laves phase was the main reason for the reduction in USR and the increment in DBTT.

Author Contributions: Conceptualization, G.Q. and D.Z.; Methodology, D.Z.; Software, C.L.; Validation, G.Q., M.Q. and Y.Y.; Formal analysis, Z.J.; Investigation, H.Z.; Resources, D.Z.; Data curation, G.Q.; Writing—original draft preparation, G.Q.; Writing—review and editing, D.Z.; Visualization, H.Z.; Supervision, C.L.; Project administration, D.Z.; Funding acquisition, D.Z. and H.Z.

Funding: This research was funded by the National Natural Science Foundation of China (No. 51874081, 51574063), the Fundamental Research Funds for the Central Universities (N150204012), and the Liaoning Province Doctoral Research Initiation Fund Guidance Project (No. 20170520079).

Conflicts of Interest: The authors declare no conflict of interest.

References

1. Gorley, M.J. Critical Assessment 12: Prospects for reduced activation steel for fusion plant. *Mater. Sci. Technol.* **2015**, *31*, 975–980. [CrossRef]
2. Kurtz, R.J.; Alamo, A.; Lucon, E.; Huang, Q.; Jitsukawa, S.; Kimura, A.; Klueh, R.L.; Odette, G.R.; Petersen, C.; Sokolov, M.A.; et al. Recent progress toward development of reduced activation ferritic/martensitic steels for fusion structural applications. *J. Nucl. Mater.* **2009**, *386–388*, 411–417. [CrossRef]
3. Tanigawa, H.; Shiba, K.; Möslang, A.; Stoller, R.E.; Lindau, R.; Sokolov, M.A.; Odette, G.R.; Kurtz, R.J.; Jitsukawa, S. Status and key issues of reduced activation ferritic/martensitic steels as the structural material for a DEMO blanket. *J. Nucl. Mater.* **2011**, *417*, 9–15. [CrossRef]
4. Lindau, R.; Moslang, A.; Rieth, M.; Klimiankou, M.; Materna-Morris, E.; Alamo, A.; Tavassoli, A.-A.F.; Cayron, C.; Lancha, A.M.; Fernandez, P.; et al. Present development status of EUROFER and ODS-EUROFER for application in blanket concepts. *Fusion Eng. Des.* **2005**, *75–79*, 989–996. [CrossRef]
5. Tan, L.; Yang, Y.; Busby, J.T. Effects of alloying elements and thermomechanical treatment on 9Cr Reduced Activation Ferritic–Martensitic (RAFM) steels. *J. Nucl. Mater.* **2013**, *442*, S13–S17. [CrossRef]
6. Tan, L.; Katoh, Y.; Tavassoli, A.-A.F.; Henry, J.; Rieth, M.; Sakasegawa, H.; Tanigawa, H.; Huang, Q. Recent status and improvement of reduced-activation ferritic-martensitic steels for high-temperature service. *J. Nucl. Mater.* **2016**, *479*, 515–523. [CrossRef]
7. Baluc, N.; Gelles, D.S.; Jitsukawa, S.; Kimura, A.; Klueh, R.L.; Odette, G.R.; van der Schaaf, B.; Yu, J. Status of reduced activation ferritic/martensitic steel development. *J. Nucl. Mater.* **2007**, *367–370*, 33–41. [CrossRef]
8. Huang, Q.; Wu, Q.; Liu, S.; Li, C.; Huang, B.; Peng, L.; Zheng, S.; Han, Q.; Wu, Y. Latest progress on R&D of ITER DFLL-TBM in China. *Fusion Eng. Des.* **2011**, *86*, 2611–2615.
9. Gao, S.; Huang, Q.; Zhu, Z.; Guo, Z.; Ling, X.; Chen, Y. Corrosion behavior of CLAM steel in static and flowing LiPb at 480 °C and 550 °C. *Fusion Eng. Des.* **2011**, *86*, 2627–2631. [CrossRef]
10. Li, C.; Huang, Q.; Wu, Q.; Liu, S.; Lei, Y.; Muroga, T.; Nagasaka, T.; Zhang, J.; Li, J. Welding techniques development of CLAM steel for test blanket module. *Fusion Eng. Des.* **2009**, *84*, 1184–1187. [CrossRef]
11. Huang, Q.; Li, J.; Chen, Y. Study of irradiation effects in China low activation martensitic steel CLAM. *J. Nucl. Mater.* **2004**, *329–333*, 268–272. [CrossRef]
12. Wu, Y. Design analysis of the China dual-functional lithium lead (DFLL) test blanket module in ITER. *Fusion Eng. Des.* **2007**, *82*, 1893–1903. [CrossRef]
13. Pan, F.; Zhang, J.; Chen, H.-L.; Su, Y.-H.; Kuo, C.-L.; Su, Y.-H.; Chen, S.-H.; Lin, K.-J.; Hsieh, P.-H.; Hwang, W.-S. Effects of Rare Earth Metals on Steel Microstructures. *Materials* **2017**, *9*, 419. [CrossRef]
14. Zhang, S.; Yu, Y.; Wang, S.; Li, H. Effects of cerium addition on solidification structure and mechanical properties of 434 ferritic stainless steel. *J. Rare Earths* **2017**, *35*, 518–524. [CrossRef]
15. Nunes, F.C.; de Almeida, L.D.; Dille, J.; Delplancke, J.-L.; Le May, I. Microstructural changes caused by yttrium addition to NbTi-modified centrifugally cast HP-type stainless steels. *Mater. Charact.* **2007**, *58*, 132–142. [CrossRef]
16. Kumar, D.; Prakash, U.; Dabhade, V.V.; Laha, K.; Sakthivel, T. Influence of Yttria on Oxide Dispersion Strengthened (ODS) Ferritic Steel. *Mater. Today* **2018**, *5*, 3909–3913. [CrossRef]
17. Li, Y.; Huang, Q.; Wu, Y.; Zheng, Y.; Zuo, Y.; Zhu, S. Effects of addition of yttrium on properties and microstructure for China Low Activation Martensitic (CLAM) steel. *Fusion Eng. Des.* **2007**, *82*, 2683–2688. [CrossRef]
18. Shi, Z.; Han, F. The microstructure and mechanical properties of micro-scale Y_2O_3, strengthened 9Cr steel fabricated by vacuum casting. *Mater. Des.* **2015**, *66*, 304–308. [CrossRef]
19. Qiu, G.; Zhan, D.; Li, C.; Qi, M.; Jiang, Z.; Zhang, H. Effects of yttrium on microstructure and properties of reduced activation ferritic-martensitic steel. *Mater. Sci. Technol.* **2018**, *34*. [CrossRef]
20. Cosgrove, G.J.; King, A.H. Adsorption, surface energy and the driving force for the migration of grain boundaries in substitutional alloys. *Mater. Sci. Eng. A* **1990**, *123*, 39–43. [CrossRef]
21. Chen, S.; Rong, L. Effect of silicon on the microstructure and mechanical properties of reduced activation ferritic/martensitic steel. *J. Nucl. Mater.* **2015**, *459*, 13–19. [CrossRef]
22. Yuan, Z.-X.; Yu, Z.-S.; Tan, P.; Song, S.-H. Effect of rare earths on the carburization of steel. *Mater. Sci. Eng. A* **1999**, *267*, 162–166. [CrossRef]

23. Dhakar, B.M.; Dwivedi, D.K.; Sharma, S.P. Studies on remelting of tungsten carbide and rare earth modified nickel base alloy composite coating. *Surf. Eng.* **2012**, *28*, 73–80. [CrossRef]
24. Yan, W.; Hu, P.; Wang, W.; Zhao, L.; Shan, Y.; Yang, K. Effect of yttrium on mechanical properties of 9Cr-2WVTa low active martensite steel. *Chin. J. Nucl. Sci. Eng.* **2009**, *29*, 50–55.
25. Panait, C.G.; Bendick, W.; Fuchsmann, A.; Gourgues-Lorenzon, A.-F.; Besson, J. Study of the microstructure of the grade 91 steel after more than 100,000h of creep exposure at 600 °C. *Int. J. Press. Vessels Pip.* **2010**, *87*, 326–335. [CrossRef]
26. Hu, X.; Huang, L.; Yan, W.; Wang, W.; Sha, W.; Shan, Y.; Yang, K. Evolution of microstructure and changes of mechanical properties of CLAM steel after long-term aging. *Mater. Sci. Eng. A* **2013**, *586*, 253–258. [CrossRef]
27. Wang, W.; Liu, S.; Xu, G.; Zhang, B.; Huang, Q. Effect of Thermal Aging on Microstructure and Mechanical Properties of China Low-Activation Martensitic Steel at 550 °C. *Nucl. Eng. Technol.* **2016**, *48*, 518–524. [CrossRef]
28. Li, Y.; Abe, H.; Li, F.; Satoh, Y.; Matsukawa, Y.; Matsunaga, T.; Muroga, T. Grain structural characterization of 9Cr–ODS steel aged at 973K up to 10,000 h by electron backscatter diffraction. *J. Nucl. Mater.* **2014**, *455*, 568–572. [CrossRef]
29. Wang, C.; Wang, M.; Shi, J.; Hui, W.; Dong, H. Effect of microstructural refinement on the toughness of low carbon martensitic steel. *Scr. Mater.* **2008**, *58*, 492–495. [CrossRef]
30. Karthikeyan, T.; Paul, V.T.; Saroja, S.; Moitra, A.; Sasikala, G.; Vijayalakshmi, M. Grain refinement to improve impact toughness in 9Cr–1Mo steel through a double austenitization treatment. *J. Nucl. Mater.* **2011**, *419*, 256–262. [CrossRef]



© 2019 by the authors. Licensee MDPI, Basel, Switzerland. This article is an open access article distributed under the terms and conditions of the Creative Commons Attribution (CC BY) license (http://creativecommons.org/licenses/by/4.0/).